Nat Hazards (2009) 48:229–243
DOI 10.1007/s11069-008-9259-x

ORIGINAL PAPER

Preliminary estimation of the tsunami hazards associated with the Makran subduction zone at the northwestern Indian Ocean

Mohammad Heidarzadeh · Moharram D. Pirooz · Nasser H. Zaker · Ahmet C. Yalciner

Received: 21 December 2007 / Accepted: 24 May 2008 / Published online: 11 June 2008

Abstract We present a preliminary estimation of tsunami hazard associated with the Makran subduction zone (MSZ) at the northwestern Indian Ocean. Makran is one of the two main tsunamigenic zones in the Indian Ocean, which has produced some tsunamis in the past. Northwestern Indian Ocean remains one of the least studied regions in the world in terms of tsunami hazard assessment. Hence, a scenario-based method is employed to provide an estimation of tsunami hazard in this region for the first time. The numerical modeling of tsunami is verified using historical observations of the 1945 Makran tsunami. Then, a number of tsunamis each resulting from a 1945-type earthquake (M_w 8.1) and spaced evenly along the MSZ are simulated. The results indicate that by moving a 1945-type earthquake along the MSZ, the southern coasts of Iran and Pakistan will experience the largest waves with heights of between 5 and 7 m, depending on the location of the source. The tsunami will reach a height of about 5 m and 2 m in northern coast of Oman and eastern coast of the United Arab Emirates, respectively.

Keywords Tsunami · Indian Ocean · Makran subduction zone (MSZ) · Deterministic tsunami hazard assessment · Numerical modeling

1 Introduction

The 2004 Indian Ocean tsunami was the deadliest tsunami in the history taking the lives of more than 230,000 people (Synolakis et al. 2007). This event emphasized the need to

M. Heidarzadeh (✉) · M. D. Pirooz
School of Civil Engineering, College of Engineering, University of Tehran,
Enghelab Ave., P.O. Box 11155-4563, Tehran, Iran
e-mail: heidarz@ut.ac.ir

N. H. Zaker
Graduate Faculty of Environment, University of Tehran, Tehran, Iran

A. C. Yalciner
Department of Civil Engineering, Ocean Engineering Research Center,
Middle East Technical University, 06531 Ankara, Turkey

assess tsunami hazards associated with the various tsunamigenic zones in the Indian Ocean basin.

A review of various tsunami catalogs (e.g., Berninghausen 1966; Murty and Rafiq 1991) reveals that tsunamis in the Indian Ocean basin have been generated by two subduction zones in this region, namely, Sunda subduction zone located offshore Indonesia and Makran subduction zone (MSZ) at the northwest of this ocean (Fig. 1) (Heidarzadeh et al. 2007, 2008b).

The Sunda subduction zone, responsible for the 2004 Indian Ocean tsunami, is the most tsunamigenic zone in the Indian Ocean which generated at least 70 tsunamis in the past (Rastogi and Jaiswal 2006). The MSZ has generated one of the deadly tsunamis in this region prior to the 2004 Indian Ocean tsunami, i.e., the Makran tsunami of 1945 with the death toll of about 4,000 people (Heck 1947). Recent studies by Heidarzadeh et al. (2008a, b) revealed that this region has experienced at least eight tsunamis in the past (Table 1 and Fig. 2), mainly generated by the earthquakes of the MSZ. Mahar and Nayyar (2006) studied the tsunami generation and propagation along the coastal zone of Makran and Karachi.

Here, we investigate the tsunami hazard associated with the MSZ using the method of deterministic tsunami hazard assessment (DTHA). The tsunami hazard caused by large subduction zone earthquakes from MSZ is considered. Landslides and volcanoes are not considered in this research for two reasons. Firstly, it is long known that the main tsunami sources are by far large subduction zone earthquakes (Synolakis 2003). Secondly, according to Heidarzadeh et al. (2008a), the most common cause for tsunami generation in the region is earthquake. Furthermore, the hazards associated with distant tsunamis originated from Sunda Arc are not studied. Okal et al. (2006a) believed that due to the geographic curvature of the Sunda Arc (Fig. 1) and taking into consideration the effect of

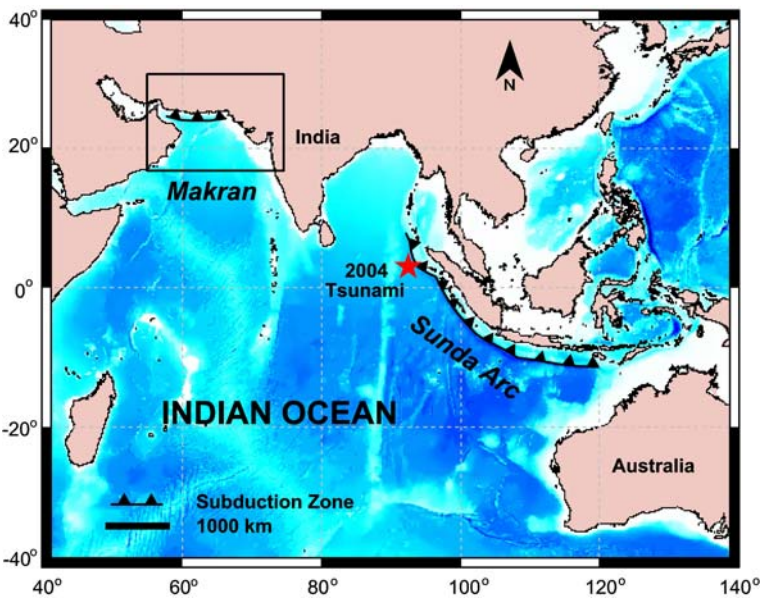

Fig. 1 Two main tsunamigenic zones in the Indian Ocean basin, namely, Makran and Sunda. The box shows the MSZ enlarged in detail in Fig. 2

Table 1 List of the tsunamis observed in the northwestern Indian Ocean (after Heidarzadeh et al. 2008a, b)

No.	Year	Location		Earthquake magnitude	Tsunami source	Loss of life	Runup (m)	CF[a]
		Longitude (°E)	Latitude (°N)					
1	326 BC	67.30	24.00	?	Earthquake	?	?	1
2	1008	60.00	25.00	?	Earthquake	1,000[b]	?	2
3	1524	Gulf of Cambay		?	Earthquake	?	?	1
4	1819	Rann of Kutch		7.5–8.25	Landslide/ volcano	>2,000[b]	?	2
5	1845	Rann of Kutch		>6	Landslide/ volcano	?	?	2
6	1897	62.30	25.00	–	Volcanic	?	?	1
7	1945	63.00	24.50	8.1–8.3	Earthquake	4,000[b]	5–12	3
8	2004	95.85	03.32	9.3	Earthquake	0[c]	0.3–3.3[c]	3

[a] Heidarzadeh et al. (2008a) assigned a confidence factor (CF) to each event whose value indicates probability of actual tsunami occurrences. They defined it as (1) probable tsunami; (2) definite tsunami but the generation mechanism and location are not certain; and (3) instrumentally recorded tsunami

[b] Both by earthquake and tsunami

[c] Recorded at the northwestern Indian Ocean

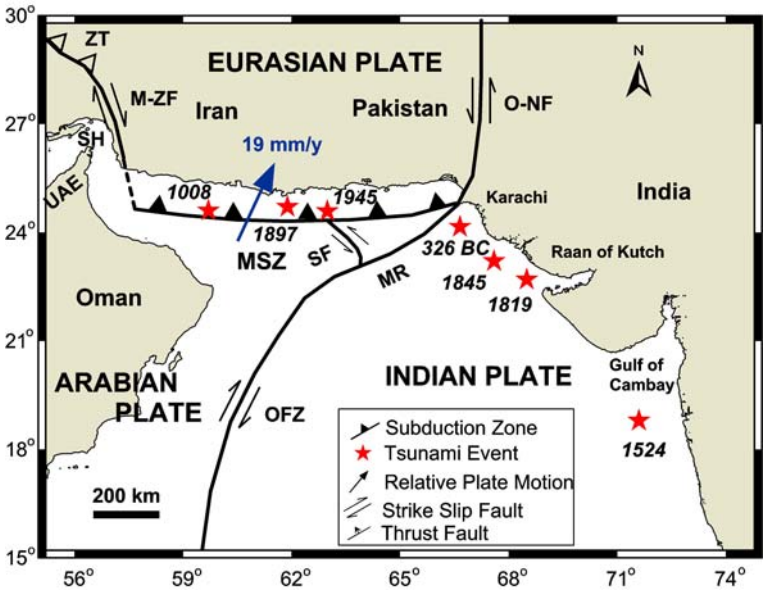

Fig. 2 Tectonic map of the MSZ along with the location of the Makran historical tsunamis. *Abbreviations*: SH, Strait of Hormoz; MSZ, Makran subduction zone; ZT, Zagros thrust; M-ZF, Minab-Zendan fault; SF, Sonne fault; MR, Murray ridge; OFZ, Owen fracture zone; O-NF, Ornach-Nal fault

directivity, tsunamis originated from Sunda Arc cannot produce large waves in the Makran region.

Different source scenarios along the MSZ are considered, and for each scenario, numerical modeling of tsunami is performed. Runup calculations are not performed here,

but the maximum positive tsunami heights (amplitudes) along the coast are calculated, which give a reasonable approximation of the runup heights (Tinti et al. 2006). These calculations provide a preliminary estimation of tsunami hazard and show which locations face the greatest threat from a large tsunami.

2 Tectonic setting

The MSZ extends east from the Strait of Hormoz in Iran to near Karachi in Pakistan with the length of about 900 km (Figs. 1 and 2). Stoneley (1974) first proposed that a subduction zone off the Makran coast forms the boundary between the Arabian and Eurasian Plates. Later, Shearman (1977) and Farhoudi and Karig (1977) presented data to support this hypothesis. Quittmeyer and Jacob (1979) stated that the seismicity in the Makran region is consistent with the interpretation of this area as an active subduction zone. According to Page et al. (1979), the raised beaches along the Makran coast confirm the tectonic model of subduction zone along this region. Recently, a comprehensive study on the tectonic and climatic evolution of the Makran region was conducted by Clift et al. (2002).

The boundaries of the MSZ are complex tectonic areas (Fig. 2). Major transpressional strike-slip system, the Ornach-Nal fault system, forms the eastern boundary of the MSZ. The Minab-Zendan fault system forms the western boundary of the MSZ as a transition zone between the Zagros continental collision and the Makran Oceanic subduction (Byrne et al. 1992). To the south, the Murry ridge delineates part of the Arabian–Indian plate boundary.

Recent studies by employing a network of 27 global position system (GPS) stations in Iran and northern Oman reveal that the subduction rate at the MSZ is about 19.5 mm y^{-1} (Vernant et al. 2004). Compared to the convergence rate of the other world's subduction zones, Makran is a relatively slow moving subduction zone. Makran is characterized by extremely shallow subduction angle (Koppa et al. 2000). Seismic reflection profiles across the MSZ showed that the MSZ includes extremely low dip angle ranging between 2° and 8° (Schluter et al. 2002). Makran has one of the largest accretionary wedges on the earth and is characterized by large sediment thickness of 7 km (Koppa et al. 2000). Unlike the other world's subduction zones, there is no trench at the location of the MSZ (Schluter et al. 2002). As for many subduction zones, active mud volcanoes are present all along the MSZ (Wiedicke et al. 2001).

3 Literature review and the present methodology

Compared to seismic hazard analysis, relatively few research works have been devoted to tsunami hazard assessment. Different researchers employed three main methods for tsunami hazard assessment as follows: (a) direct statistical tsunami hazard assessment (DSTHA), (b) DTHA (Geist and Parsons 2006), and (c) probabilistic tsunami hazard assessment (PTHA).

DSTHA includes direct assessment of tsunami hazards in a particular region based on tsunami catalogs. Using actual data of tsunamis in a particular coastline, some relations, such as earthquake magnitude–tsunami height, will be obtained. Because DSTHA is based on tsunami catalogs, it only can be applied to regions with sufficient historical data of tsunami. In addition, application of statistical equations linking tsunami height with earthquake magnitude may not be without deficiency, because the actual tsunami wave

height at the coast would be strongly influenced by the local bathymetry and topography. Among researchers who used DSTHA are Pelinovsky (1999), Tinti and Maramai (1999), Kulikov et al. (2005), Orfanogiannaki and Papadopoulos (2007).

When data of historical tsunamis for a particular site are lacking, tsunami hazard can be calculated using either DTHA or PTHA. However, most tsunami hazard assessments in the past have been performed using DTHA (Geist and Parsons 2006). DTHA is based on adopting characteristic scenarios considering the largest event known to have hit the area of interest in the past and to simulate this event through numerical modeling (Geist and Parsons 2006). The tsunami scenarios can either be based on historic events or hypothetical ones (Geist and Parsons 2006). In cases where deterministic scenarios are not based on historic events, there may be a tendency to use maximum credible tsunami for a given region (Geist and Parsons 2006). Further examples of application of DTHA can be found in Tinti and Armigliato (2003), Yalciner et al. (2004), Legg et al. (2004), Okal et al. (2006b).

The PTHA is similar to seismic hazard assessment (Lin and Tung 1982). This method uses a combination of probability evaluation for offshore earthquake occurrence and numerical modeling of tsunami waves to determine the probability of having a tsunami, whose maximum water elevation exceeds a certain value at a coastal site. Geist and Parsons (2006) believed whereas probabilistic analysis of tsunami hazards yields information on likelihood of tsunami events, the results of PTHA may be difficult to interpret. Further application of PTHA can be found in Annaka et al. (2007) and Liu et al. (2007).

Here we employ the method of DTHA for Makran for the following reasons. First, the historical data of tsunami in the Makran region are rather poor. The runup records are known only for two events of 1945 and 2004. Therefore, the direct statistical method (DSTHA) cannot yield useful results. Second, establishment of specific tsunamigenic zones offshore Makran coast is difficult because only one event is instrumentally recorded. This makes the application of PTHA problematic. Furthermore, as this is the first study on the Makran tsunami hazard assessment, there is a preference for the deterministic method over the probabilistic one, because the results of the former method are relatively easier to interpret and can more effectively be used by civil defense authorities. The present deterministic methodology includes the following steps: (1) selecting the characteristic earthquake, (2) modeling ocean-floor displacement field, and (3) numerical modeling of tsunami.

4 The components of the present method

4.1 The characteristic earthquake

The 1945 Makran earthquake (M_w 8.1–8.3) is considered to be the characteristic earthquake for tsunami hazard assessment, because (1) it is the most destructive event in the region, among those known; (2) it has been the largest earthquake occurred in this region; and (3) there is sufficient information on the seismic parameters.

Byrne et al. (1992) reported seven large earthquakes ($M_w > 7$) in the MSZ in the past 500 years. However, they concluded that none of these events were as large as the 1945 one. Byrne et al. (1992) calculated the source parameters of the 1945 earthquake as seismic moment of 1.8×10^{21} N m, moment magnitude of M_w 8.1, rupture length of 100–150 km, rupture width of about 100 km, slip on the fault surface of 6–7 m, strike angle of 246°, dip angle of 7°, slip angle of 89°, and depth of 27 ± 3 km. Byrne et al. (1992) believed that similar events would be expected to repeat at least every 175 years in eastern Makran.

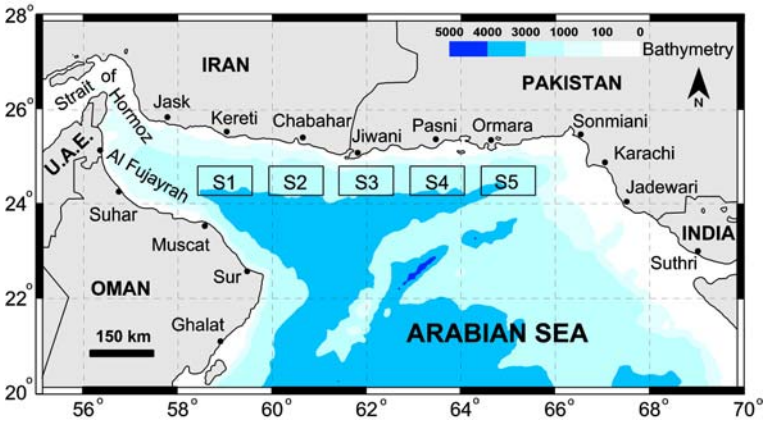

Fig. 3 Five earthquake scenarios (S1–S5) considered in this study along with the bathymetry of the MSZ and major coastal cities

Page et al. (1979) estimated that the recurrence of a similar 1945-type earthquake along the MSZ is approximately 125–250 years. Quittmeyer and Jacob (1979) reported the intensity (in modified mercally scale), surface magnitude (M_s), and rupture length of the 1945 event to be 10, 8, and 150–200 km, respectively. Several authors reported that this earthquake produced 2 m of uplift on the ocean floor (e.g., Ambraseys and Melville 1982).

Here we moved the earthquake's epicenter along the MSZ to define different scenarios for tsunami modeling. Based on the seismic parameters of the 1945 event, five earthquakes spaced evenly along the MSZ from Karachi to the Strait of Hormoz have been considered because any similar earthquake is capable of rupturing about 150–200 km of the plate boundary (Fig. 3).

4.2 Modeling of ocean floor displacement field and verification

The tsunami modeling process can be divided into three parts: generation, propagation, and runup (Synolakis 2003). Generation modeling forms the first stage in the modeling of tsunami and includes the calculation of the initial disturbance of the ocean surface due to the earthquake-triggered deformation of the seafloor. A hydrodynamic model takes the initial wave to model the propagation and runup of the tsunami waves.

Most studies of tectonic tsunamis use Mansinha and Smylie's (1971) formula or Okada's (1985) analytical formula to predict seafloor displacement due to an earthquake and to model initial water displacement (Legg et al. 2004). Here, the algorithm of Mansinha and Smylie (1971) is used to calculate the seafloor deformation. This algorithm calculates the sea floor deformation using input seismic parameters. Only one rectangular source is considered for each scenario because the MSZ is relatively straight (Fig. 2).

We varied the rupture length, width, and slip in order to reproduce the vertical displacement of 2 m on the ocean floor. The dip, strike, slip angles, and the depth of the earthquake were kept constant. However, in all cases the seismic moment of 1.8×10^{21} N m was maintained. It is well known that for a rectangular fault of length L and width W, the seismic moment (M_0) is defined as $M_0 = \mu LWD$ (Kanamori and Anderson 1975) in which μ is the rigidity of the earth (about 3×10^{10} N m^{-2} for the Makran region; Bayer et al. 2006), L and W are the length and width of the rupture, respectively, and D is the amount of slip. A summary of dislocation modeling efforts is presented in Table 2. According to this table,

Table 2 Results of the dislocation modeling using variable rupture length, width, and slip for the Makran earthquake of 1945

No.	Dip (°)	Slip (°)	Strike (°)	Depth (km)	Length (km)	Width (km)	Slip (m)	Moment (N m)	Uplift (m)
1	7	89	246	27	150	75	5.3	1.8×10^{21}	1.7
2	7	89	246	27	150	70	5.7	1.8×10^{21}	1.8
3	7	89	246	27	150	65	6.15	1.8×10^{21}	1.9
4	7	89	246	27	140	75	5.7	1.8×10^{21}	1.8
5	7	89	246	27	140	70	6.1	1.8×10^{21}	1.9
6	7	89	246	27	120	80	6.25	1.8×10^{21}	2.0
7	7	89	246	27	130	75	6.15	1.8×10^{21}	1.9
8	7	89	246	27	130	70	6.6	1.8×10^{21}	2.0

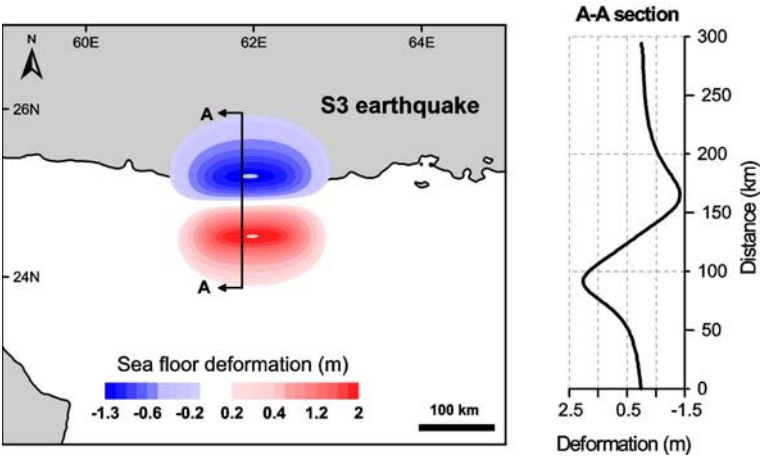

Fig. 4 Result of the tsunami generation modeling for S3 showing a 2D in plan view of the seafloor deformation and a cross section perpendicular to the strike of the dislocation

the seismic parameters presented in the last row were used for tsunami generation modeling. The displacement field of the earthquake for the case of S3 is shown in Fig. 4.

4.3 Modeling of tsunami and verification

The numerical model TUNAMI-N2 is used for simulation of propagation and coastal amplification of tsunami. The model was originally authored by Professors Nobuo Shuto and Fumihiko Imamura of the Disaster Control Research Center in Tohoku University (Japan) through the Tsunami Inundation Modeling Exchange (TIME) program (Goto et al. 1997; Yalciner et al. 2002). TUNAMI-N2 is one of the key tools for developing studies for propagation and coastal amplification of tsunamis in relation to different initial conditions. It solves nonlinear shallow water equations in Cartesian coordinates using the leap-frog scheme of finite differences (Yalciner et al. 2004). Also, a similar methodology is used in the numerical model of method of splitting tsunami (MOST) developed by Titov and Synolakis (1997, 1998). TUNAMI-N2 and MOST are the only two existing nonlinear shallow water codes, validated with laboratory and field data (Yeh et al. 1996).

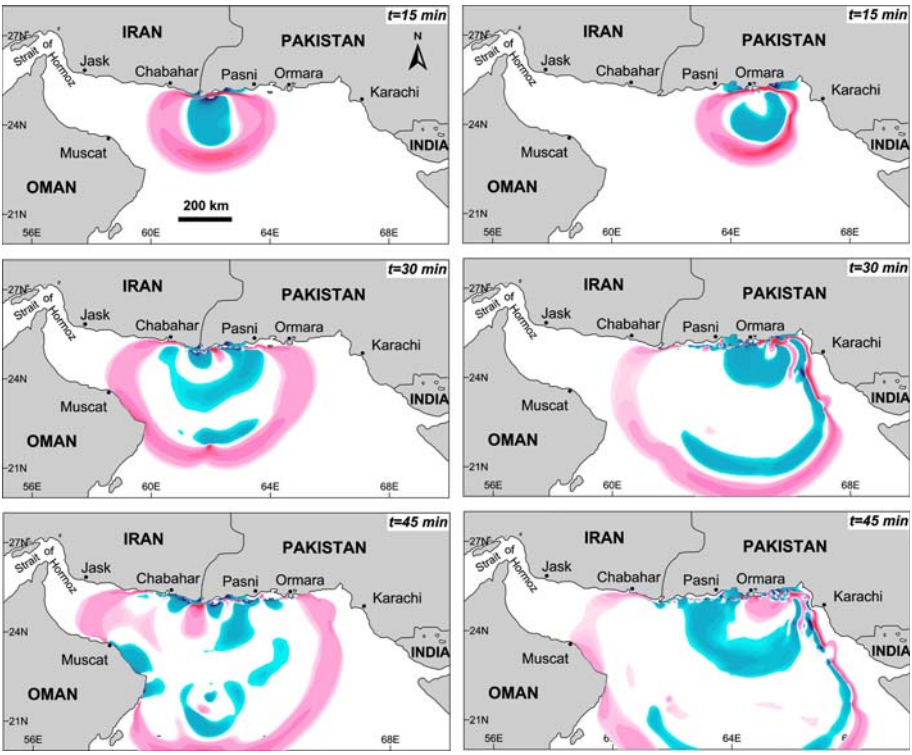

Fig. 5 Snapshots of the tsunami simulation after t = 15, 30, and 45 min for the cases of S3 (left column) and S5 (right column) scenarios

In this study, we apply bathymetry data provided through general bathymetric chart of the oceans (GEBCO) digital atlas (IOC et al. 2003). The total number of grid points in the computational domain was 369,852 consisting of 833 × 444 points. The time step was 1.0 s to satisfy the stability condition. The duration time of wave propagation was 5 h. Figure 5 shows examples of snapshots of the water surface displacement at times t = 15, 30, and 45 min for the cases of S3 and S5 scenarios.

To verify the tsunami propagation modeling, we compare the modeling results with the actual data of the 1945 Makran tsunami. Among five different scenarios considered in this study, the epicenter of the S4 coincides with that of the 1945 event, and thus, we compare the wave heights resulting from S4 scenario with the actual data of the 1945 event.

The data of Makran 1945 tsunami wave heights on the coastlines are rather poor, and no tide gauge data is available. However, we were able to collect some data about tsunami wave heights on various Makran coasts. Based on Page et al. (1979), the 1945 tsunami reached a height of 7–10 m in Pasni. According to Ambraseys and Melville (1982), tsunami wave height in Pasni was about 4–5 m and was about 1.5 m high in Karachi. Also, they reported that the tsunami was observed along Makran coasts of Iran and Oman. However, no damage and loss of life were reported from these coasts. Among reports, the report by Ambraseys and Melville (1982) seems more reliable since their report is based on the detailed research on the historical earthquakes in the region using specialized methods to discriminate between reliable and unreliable historical accounts.

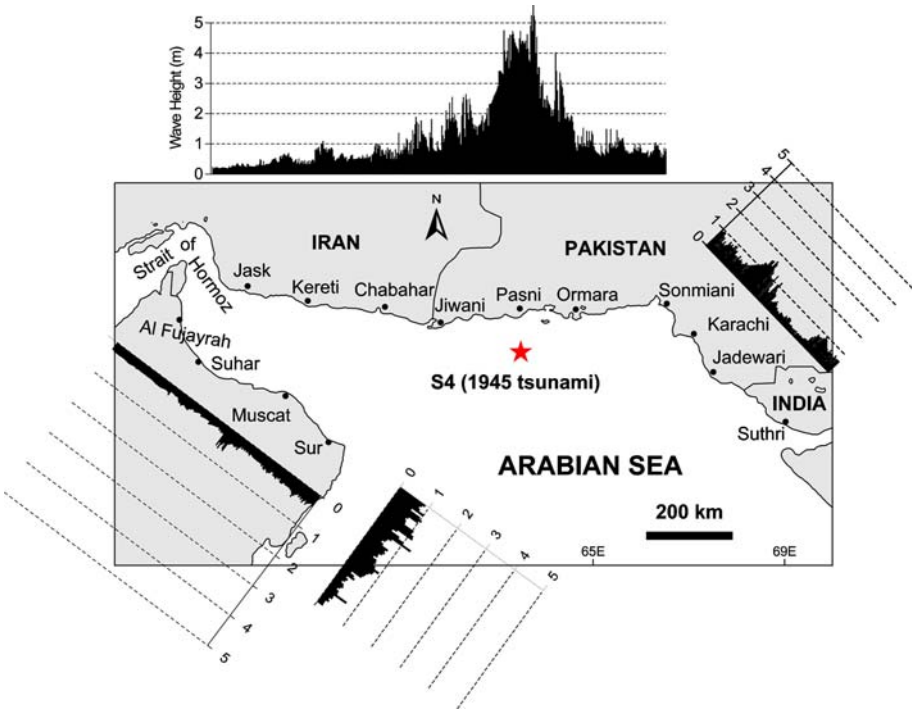

Fig. 6 Distribution of maximum positive tsunami wave heights in various Makran coasts due to the S4 scenario which is similar to the Makran tsunami of 1945

Figure 6 presents the results of numerical modeling of tsunami for the S4. As can be seen, the distribution of tsunami wave height along various Makran coasts reproduces most feathers of the historical observations during the 1945 event. Our numerical model successfully reproduced the wave height of between 4 and 5 m at Pasni as well as 1.5 m in Karachi. In addition, Fig. 6 shows that the simulated wave heights are less than 1 m at the southern coast of Iran and northern coast of Oman; thus, it is reasonable that there is little information about the effects of Makran tsunami of 1945 on these coasts.

4.4 Runup modeling

To further examine the accuracy of the results, we performed runup modeling for one coastal site (Pasni) using high resolution bathymetry and topography data. In addition, such modeling gives important information about the evolution of tsunami in coastal areas, e.g., the maximum horizontal penetration of tsunami in dry land. The modeling practice presented in the Sect. 4.3 is repeated to calculate the runup heights in Pasni.

The nested grid version of TUNAMI-N2 (known as TUNAMI-N3) was employed. It solves the linear form of the long-wave equations in spherical coordinates in the largest domain (the deep sea) and nonlinear shallow-water equations in Cartesian coordinates in smaller domains with finer grids. A set of four-level nested grid (grid set of ABCD in Fig. 7), where the grid resolution increases in the coastal areas, was used. The first grid, entitled A, covers the entire MSZ between 55–70°E and 20–28°N at a resolution of about 2,500 m. For the region entitled D, where inundation of tsunami in dry land is permitted,

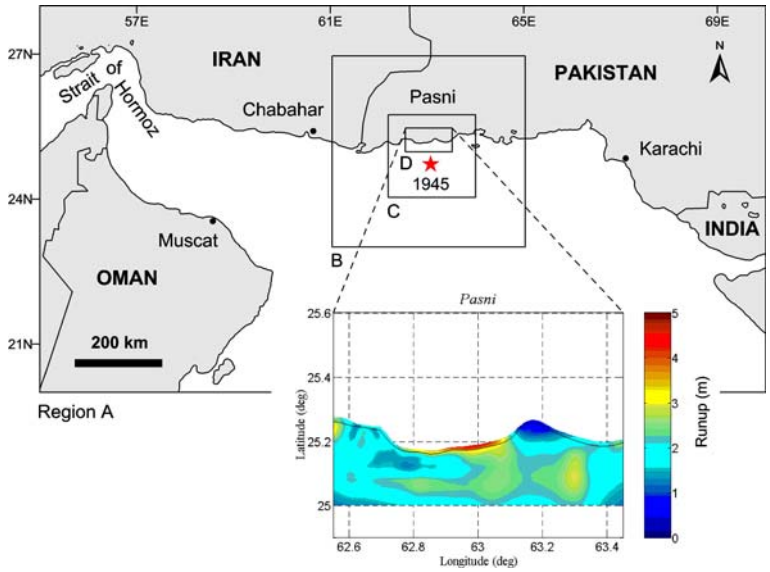

Fig. 7 Result of detailed runup modelling performed in Pasni due to the Makran tsunami of 1945

the resolution of the bathymetry and topography data was about 100 m. Kukowski et al. (2001) developed detailed bathymetric images of the MSZ.

The result of the runup modeling in Pasni is shown in Fig. 7. The maximum simulated runup height is about 5 m, which is in agreement with both the historical observations and the results of maximum tsunami heights along the coast presented in the Sect. 4.3. In addition, Fig. 7 shows that the maximum horizontal penetration of the 1945 tsunami in dry land is about 1 km.

5 Results

Figures 8 and 9 present the results of the tsunami modeling for all the five scenarios. Figure 8a–e shows the maximum wave height of the tsunami as it travels in the northwestern Indian Ocean. Since the energy of a tsunami is a function of its wave height, these figures also show the propagation direction of the tsunami's energy. Most of the tsunami's energy travels perpendicular to the strike of the fault which is evident from the theory of directivity (Ben-Menahem and Rosenman 1972). Due to this effect, most of the energy propagates in the north–south direction (Fig. 8) focusing on the southern coasts of Iran and Pakistan in the north direction and also on the northern coast of Oman and eastern coast of United Arab Emirates (UAE) at the south direction. Furthermore, tsunamis originating from the middle and eastern part of the MSZ have minor effects on the Omani and Emirian coasts (S3, S4, and S5 scenarios—Fig. 8c–e). This result is in agreement with the observed impact of the 1945 tsunami whose location was close to the S4 scenario.

In the case of S1 (Fig. 8a), whose epicenter is located in the westernmost of the MSZ, most of the tsunami's wave height remains close to the coasts of Iran, Oman, and UAE, and only a small part of it affects other coasts. By contrast, the S5 scenario, at the easternmost, produces only large waves on the Pakistani coast. The location of the S4 scenario is close

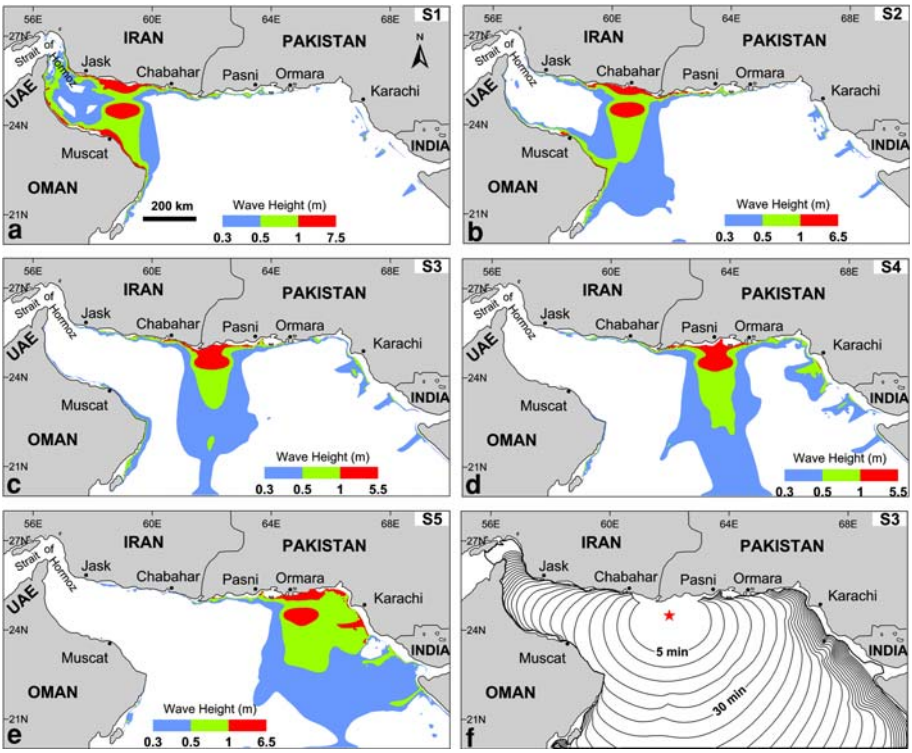

Fig. 8 The maximum positive tsunami wave height at various locations for different scenarios (graphs **a**–**e**). Graph **f** shows the tsunami travel time for S3 scenario. In this graph, the time interval between two neighboring contour is 5 min

to the November 1945 tsunami near Pasni. As mentioned before, it affected a similar area with similar wave heights. The three scenarios of S2, S3, and S4 seriously affect large parts of the Makran coast. However, it is clear from the maximum positive tsunami wave height (Fig. 8) that all the five scenarios are capable of affecting the entire Makran coasts, although the wave height is less than 50 cm at distant coasts.

Figure 8f presents an example of the tsunami travel time chart for the case of S3 scenario. It shows that the travel time curves are very close to each other near the Strait of Hormoz and western coast of India. This is due to shallow water of these regions as shown in Fig. 3. According to this graph, in the case of S3 scenario, the first tsunami wave reaches the northern and southern coasts of Makran in about 10 and 25 min, respectively. However, modeling results reveal that the largest tsunami wave arrives in about 20 min after the earthquake at the northern coast of Makran. Therefore, if we suppose at least 5 min in order to take refuge from tsunami, emergency services have only about 15-min time to detect and measure the event and issue the required warning to the coastal communities.

Figure 9 shows the maximum positive tsunami wave height for all the five scenarios. The northern coast of Makran experiences the largest waves for all the scenarios. Along this coast, the maximum amplitude of tsunami waves ranges from 5 to 7 m, depending on the location of the source. The waves on the Iranian coast are slightly larger than those at the Pakistani coast, which can be attributed to the local bathymetry and topography.

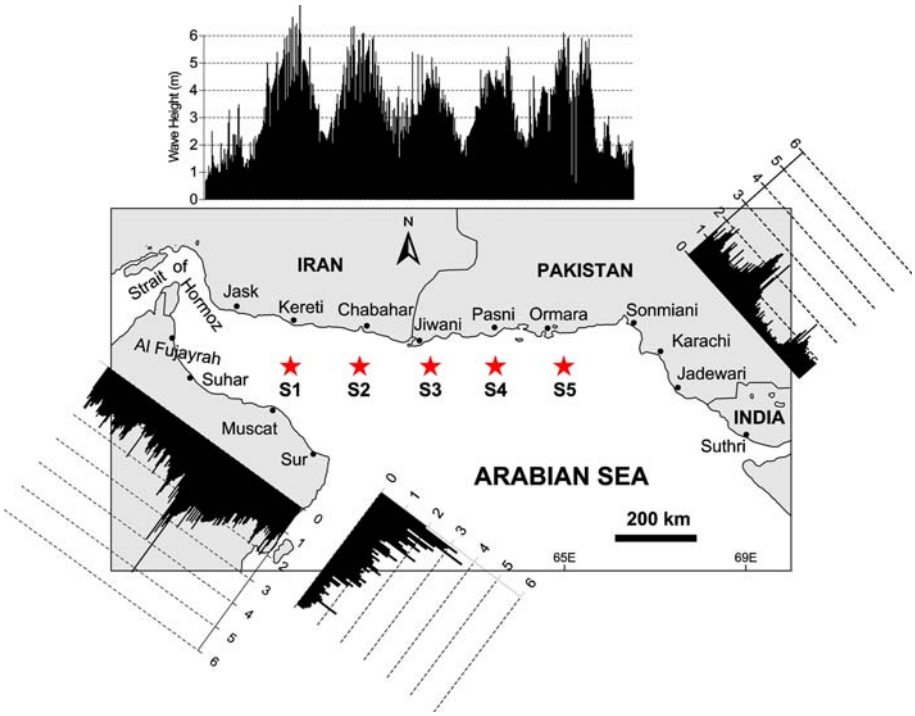

Fig. 9 Distribution of the maximum positive tsunami wave heights along various Makran coasts for all the five scenarios

In northern Oman, where the average amplitude of the tsunami is about 1.5 m, Muscat and its adjacent areas experience relatively huge amplitude of up to 5 m. A similar situation can be observed in Karachi and also in the eastern Oman headland, south of Sur. In these populated coastal cities, a significant amplification of the tsunami waves is evident. In Fig. 9, the tsunami wave height in Karachi and Muscat is twice that in adjacent areas. Despite Emirian coast is not known for its tsunami hazard, Fig. 9 reveals that the tsunami wave height in eastern coast of UAE (e.g., in Al Fujayrah) is up to about 2 m, which indicates that the tsunami hazard of this region cannot be neglected.

6 Discussion

TUNAMI-N2 treats the coastline as a vertical wall, and hence, flooding was not permitted. Therefore, it is possible that our results underestimate or overestimate the runup heights in some areas due to hydrodynamic effects during wave evolution on the actual beach topography.

In addition, the results are obtained considering an M_w 8.1 earthquake as tsunami source for each of the five scenarios. Different studies reveal that Makran exhibits strong variation in seismicity between its eastern and western segments (Quittmeyer and Jacob 1979; Byrne et al. 1992). While a 1945-type earthquake can occur every about 150–250 years in eastern Makran (Page et al. 1979; Byrne et al. 1992), the western Makran has no clear record of historic great earthquakes and has not experienced a large earthquake at least in the past

500 years (Byrne et al. 1992). Hence, Byrne et al. (1992) concluded that either entirely aseismic subduction occurs in the western Makran or the plate boundary is currently locked and experiences great earthquakes with long repeat times. Therefore, it is necessary to take into consideration this fact for assessing tsunami hazard in western Makran or developing inundation maps for coastal areas in this region.

7 Conclusion

A number of tsunamis, each resulting from a 1945-type earthquake (M_w 8.1) and spaced evenly along the MSZ, were simulated in order to provide a preliminary estimation of tsunami hazard faced by different Makran coasts. The results of numerical modeling of tsunami were verified by comparing with historical observations of the 1945 earthquake and tsunami. The following conclusions can be deduced:

(1) Most of the tsunami's energy in the MSZ propagates in the north–south direction focusing on the southern coasts of Iran and Pakistan and also on the northern coast of Oman and eastern coast of UAE.
(2) Southern coasts of Iran and Pakistan experience the largest waves with heights of about 5–7 m depending on the location of tsunami source.
(3) Northern coast of Oman and eastern coast of UAE experience wave heights of up to about 5 and 2 m, respectively. It can be concluded that the tsunami hazard of Emirian coast cannot be neglected.
(4) The results reveal significant wave amplification in the two most populated coastal cities in the region, namely, Karachi and Muscat.
(5) Due to the effect of directivity, tsunamis originating from the middle and eastern part of the MSZ have minor effects on the Omani and Emirian coasts.
(6) Since Makran is naturally enclosed in three directions, any tsunami from MSZ can affect the entire region.
(7) The largest tsunami wave arrives about 20 min after the earthquake at the nearest coast. Therefore, emergency services have about 15-min time to detect and measure the event and issue the required warning.
(8) Runup modeling performed in Pasni revealed that the maximum inundation distance of tsunami in dry land was about 1 km due to the 1945 Makran tsunami.

Acknowledgments The long wave propagation models, TUNAMI-N2 and TUNAMI-N3, used in this study are registered copyright of Professors F. Imamura, Ahmet C. Yalciner, and C. E. Synolakis. The Intergovernmental Oceanographic Commission (IOC) of UNESCO is thanked for funding the first author's participation in the first international tsunami modeling course held in Kuala Lumpur, Malaysia, in May 2006. The first author would like to extend his sincere gratitude to Professor Emile A. Okal (Northwestern University, IL, USA) and Professor Costas E. Synolakis (University of Southern California, CA, USA) for their fruitful discussions during the Malaysia international course. This manuscript benefited from constructive reviews by two anonymous reviewers. We are sincerely grateful to the reviewers for comments that improved this article.

References

Ambraseys NN, Melville CP (1982) A history of Persian earthquakes. Cambridge University Press, Britain

Annaka T, Satake K, Sakakiyama T, Yanagisawa K, Shuto N (2007) Logic-tree approach for probabilistic tsunami hazard analysis and its applications to the Japanese coasts. Pure Appl Geophys 164:577–592. doi:10.1007/s00024-006-0174-3

Bayer R, Chery J, Tatar M, Vernant P, Abbassi M, Masson F et al (2006) Active deformation in Zagros–Makran transition zone inferred from GPS measurements. Geophys J Int 165:373–381. doi:10.1111/j.1365-246X.2006.02879.x

Ben-Menahem A, Rosenman M (1972) Amplitude patterns of tsunami waves from submarine earthquakes. J Geophys Res 77:3097–3128. doi:10.1029/JB077i017p03097

Berninghausen WH (1966) Tsunamis and seismic seiches reported from regions adjacent to the Indian Ocean. Bull Seismol Soc Am 56(1):69–74

Byrne DE, Sykes LR, Davis DM (1992) Great thrust earthquakes and aseismic slip along the plate boundary of the Makran subduction zone. J Geophys Res 97(B1):449–478. doi:10.1029/91JB02165

Clift PD, Kroon D, Gaedicke C, Craig J (2002) The tectonic and climatic evolution of the Arabian Sea region. Geol Soc Lond Spec Publ 195:532 pp

Farhoudi G, Karig DE (1977) The Makran of Iran and Pakistan as an active arc system. Abstr Eos Trans AGU 58:446

Geist EL, Parsons T (2006) Probabilistic analysis of tsunami hazards. Nat Hazards 37:277–314. doi:10.1007/s11069-005-4646-z

Goto C, Ogawa Y, Shuto N, Imamura F (1997) Numerical method of tsunami simulation with the Leap-Frog Scheme (IUGG/IOC Time Project), IOC Manual, UNESCO, No. 35

Heck NH (1947) List of seismic sea waves. Bull Seismol Soc Am 37(4):269–286

Heidarzadeh M, Pirooz MD, Zaker NH, Mokhtari M (2007) Evaluating the potential for tsunami generation in southern Iran. Int J Civ Eng 5(4):312–329

Heidarzadeh M, Pirooz MD, Zaker NH, Yalciner AC, Mokhtari M, Esmaeily A (2008a) Historical tsunami in the Makran subduction zone off the southern coasts of Iran and Pakistan and results of numerical modeling. Ocean Eng 35(8&9):774–786

Heidarzadeh M, Pirooz MD, Zaker NH, Yalciner AC (2008b) Assessment of historical tsunamis in the northwestern Indian Ocean using detailed archival research and hydrodynamic modeling (manuscript in preparation)

IOC, IHO, BODC (2003) Centenary edition of the GEBCO digital atlas, published on CD-ROM on behalf of the Intergovernmental Oceanographic Commission and the International Hydrographic Organization as part of the general bathymetric chart of the oceans. British oceanographic data centre, Liverpool

Kanamori H, Anderson DL (1975) Theoretical basis of some empirical relations in seismology. Bull Seismol Soc Am 65(5):1073–1095

Koppa C, Fruehn J, Flueh ER, Reichert C, Kukowski N, Bialas J et al (2000) Structure of the Makran subduction zone from wide-angle and reflection seismic data. Tectonophysics 329:171–191. doi:10.1016/S0040-1951(00)00195-5

Kukowski N, Schillhorn T, Huhn K, von Rod U, Husen S, Flueh ER (2001) Morphotectonics and mechanics of the Central Makran accretionary wedge off Pakistan. Mar Geol 173:1–19. doi:10.1016/S0025-3227(00)00167-5

Kulikov EA, Rabinovich AB, Thomson RE (2005) Estimation of tsunami risk for the coasts of Peru and Northern Chile. Nat Hazards 35:185–209. doi:10.1007/s11069-004-4809-3

Legg MR, Borrero JC, Synolakis CE (2004) Tsunami hazards associated with the Catalina fault in southern California. Earthq Spectra 20(3):1–34. doi:10.1193/1.1773592

Lin IC, Tung CC (1982) A preliminary investigation of tsunami hazard. Bull Seismol Soc Am 72(6):2323–2337

Liu Y, Santos A, Wang SM, Shi Y, Liu H, Yuen DA (2007) Tsunami hazards along Chinese coast from potential earthquakes in South China Sea. Phys Earth Planet Inter 163(1–4):233–244. doi:10.1016/j.pepi.2007.02.012

Mahar GA, Nayyar ZA (2006) Tsunami generation and propagation among the coastal zone of Makran and Karachi. In: Proceedings of the international conference on advances in space technologies, Islamabad, 2–3 Sept 2006

Mansinha L, Smylie DE (1971) The displacement field of inclined faults. Bull Seismol Soc Am 61(5):1433–1440

Murty T, Rafiq M (1991) A tentative list of tsunamis in the marginal seas of the north Indian Ocean. Nat Hazards 4:81–83. doi:10.1007/BF00126560

Okada Y (1985) Surface deformation due to shear and tensile faults in a half space. Bull Seismol Soc Am 75(4):1135–1154

Okal EA, Borrero JC, Synolakis CE (2006b) Evaluation of tsunami risk from regional earthquakes at Pisco, Peru. Bull Seismol Soc Am 96(5):1634–1648. doi:10.1785/0120050158

Okal EA, Fritz HM, Raad EP, Synolakis CE, Al-Shijbi Y, Al-Saifi M (2006a) Oman field survey after the December 2004 Indian Ocean tsunami. Earthq Spectra 22(S3):S203–S218. doi:10.1193/1.2202647

Orfanogiannaki K, Papadopoulos GA (2007) Conditional probability approach of the assessment of tsunami potential: application in three tsunamigenic regions of the Pacific Ocean. Pure Appl Geophys 164: 593–603. doi:10.1007/s00024-006-0170-7

Page WD, Alt JN, Cluff LS, Plafker G (1979) Evidence for the recurrence of large-magnitude earthquakes along the Makran coast of Iran and Pakistan. Tectonophysics 52:533–547. doi:10.1016/0040-1951(79)90269-5

Pelinovsky E (1999) Preliminary estimates of tsunami danger for the northern part of the Black Sea. Phys Chem Earth A 24(2):175–178. doi:10.1016/S1464-1895(99)00015-0

Quittmeyer RC, Jacob KH (1979) Historical and modem seismicity of Pakistan, Afghanistan, northwestern India, and southeastern Iran. Bull Seismol Soc Am 69(3):773–823

Rastogi BK, Jaiswal RK (2006) A catalog of tsunamis in the Indian Ocean. Sci Tsunami Hazards 25(3): 128–143

Schluter HU, Prexl A, Gaedicke C, Roeser H, Reichert C, Meyer H, von Daniels C (2002) The Makran accretionary wedge: sediment thicknesses and ages and the origin of mud volcanoes. Mar Geol 185:219–232. doi:10.1016/S0025-3227(02)00192-5

Shearman DJ (1977) The geological evolution of southern Iran, the report of the Iranian Makran expedition. Geogr J 142:393–410. doi:10.2307/1795293

Stoneley R (1974) Evolution of the continental margins bounding a former Tethys. In: Burk CA, Drake CL (eds) The geology of continental margins. Springer, New York, pp 889–903

Synolakis CE (2003) Tsunami and seiche. In: Chen WF, Scawthorn C (eds) Earthquake engineering handbook, Chapter 9. CRC Press, pp 1–90

Synolakis CE, Okal EA, Bernard E (2007) The megatsunami of December 26, 2004. Bridge 35(2):26–35

Tinti S, Armigliato A (2003) The use of scenarios to evaluate the tsunami impact in southern Italy. Mar Geol 199:221–243. doi:10.1016/S0025-3227(03)00192-0

Tinti S, Maramai A (1999) Large tsunamis and tsunami hazard from the new Italian tsunami catalog. Phys Chem Earth A 24(2):151–156. doi:10.1016/S1464-1895(99)00011-3

Tinti S, Armigliato A, Manucci A, Pagnoni G, Zaniboni F, Yalciner AC, Altinok Y (2006) The generating mechanisms of the August 17, 1999 Izmit Bay (Turkey) tsunami: regional (tectonic) and local (mass instabilities) causes. Mar Geol 225:311–330. doi:10.1016/j.margeo.2005.09.010

Titov VV, Synolakis CE (1997) Extreme inundation flow during the Hokkaido-Nansei-Oki tsunami. Geophys Res Lett 24:1315–1318. doi:10.1029/97GL01128

Titov VV, Synolakis CE (1998) Numerical modeling of tidal wave runup. J Waterw Port Cost Ocean Eng B 124:157–171. doi:10.1061/(ASCE)0733-950X(1998)124:4(157)

Vernant P, Nilforoushan F, Hatzfeld D, Abbasi MR, Vigny C, Masson F, Nankali H, Martinod J, Ashtiani A, Bayer R, Tavakoli F, Chéry J (2004) Present-day crustal deformation and plate kinematics in the middle east constrained by GPS measurements in Iran and northern Oman. Geophys J Int 157:381–398. doi:10.1111/j.1365-246X.2004.02222.x

Wiedicke M, Neben S, Spiess V (2001) Mud volcanoes at the front of the Makran accretionary complex, Pakistan. Mar Geol 172:57–73. doi:10.1016/S0025-3227(00)00127-4

Yalciner AC, Alpar B, Altinok Y, Ozbay I, Imamura F (2002) Tsunamis in the sea of Marmara, historical documents for the past, models for the future. Mar Geol 190:445–463. doi:10.1016/S0025-3227(02)00358-4

Yalciner AC, Pelinovsky E, Talipova T, Kurkin A, Kozelkov A, Zaitsev A (2004) Tsunamis in the Black Sea: comparison of the historical, instrumental, and numerical data. J Geophys Res 109(12):2003–2113. doi:10.1029/2003JC002113

Yeh H, Liu P, Synolakis CE (1996) Long wave runup models. World Scientific Publication Company, London, 403 pp